GALILEO ULTRAVIOLET SPECTROMETER EXPERIMENT

C. W. HORD, W. E. McCLINTOCK, A. I. F. STEWART, C. A. BARTH, L. W. ESPOSITO, G. E. THOMAS,

Laboratory for Atmospheric and Space Physics, University of Colorado at Boulder, Boulder, CO 80309–0392, U.S.A.

B. R. SANDEL, D. M. HUNTEN, A. L. BROADFOOT, D. E. SHEMANSKY,

Lunar and Planetary Laboratory, 901 Gould–Simpson Building, University of Arizona, Tucson, AZ 85721, U.S.A.

J. M. AJELLO, A. L. LANE, and R. A. WEST

Jet Propulsion Laboratory, California Institute of Technology, Pasadena, CA 91109, U.S.A.

Abstract. The Galileo ultraviolet spectrometer experiment uses data obtained by the Ultraviolet Spectrometer (UVS) mounted on the pointed orbiter scan platform and from the Extreme Ultraviolet Spectrometer (EUVS) mounted on the spinning part of the orbiter with the field of view perpendicular to the spin axis. The UVS is a Ebert–Fastie design that covers the range 113–432 nm with a wavelength resolution of 0.7 nm below 190 and 1.3 nm at longer wavelengths. The UVS spatial resolution is 0.4 deg × 0.1 deg for illuminated disc observations and 1 deg × 0.1 deg for limb geometries. The EUVS is a Voyager design objective grating spectrometer, modified to cover the wavelength range from 54 to 128 nm with wavelength resolution 3.5 nm for extended sources and 1.5 nm for point sources and spatial resolution of 0.87 deg × 0.17 deg. The EUVS instrument will follow up on the many Voyager UVS discoveries, particularly the sulfur and oxygen ion emissions in the Io torus and molecular and atomic hydrogen auroral and airglow emissions from Jupiter. The UVS will obtain spectra of emission, absorption, and scattering features in the unexplored, by spacecraft, 170–432 nm wavelength region. The UVS and EUVS instruments will provide a powerful instrument complement to investigate volatile escape and surface composition of the Galilean satellites, the Io plasma torus, micro- and macro-properties of the Jupiter clouds, and the composition structure and evolution of the Jupiter upper atmosphere.

1. Introduction

The Galileo Ultraviolet Spectrometer investigation will use data obtained by two instruments. The Ultraviolet Spectrometer (UVS) covers the wavelength range from 113 to 432 nm and was the original instrument selected for the Galileo Orbiter. The Extreme Ultraviolet Spectrometer (EUVS) was added to the Orbiter payload after the Challenger accident in 1986. A joint effort by the Universities of Colorado and Arizona culminated in the EUVS instrument, a modified version of the Voyager Ultraviolet Spectrometer, covering the wavelength region from 54 to 128 nm.

Primary objectives of the investigation are to understand physical processes occurring in: (1) the upper atmosphere of Jupiter; (2) the Io plasma torus; (3) the volatile gases escaping from Galilean satellites. The surface scattering properties of Jupiter's moons will be investigated. The spectral features of H and H_2 in the Jupiter aurora and airglow investigated by the Voyager Ultraviolet Spectrometer form a solid point of departure for the investigation of the composition and thermal structure of the upper atmosphere. Sulfur and oxygen ions discovered by Voyager provide the tracers to understand the time evolution of volcanic gases from Io in their transit through the plasma torus and ultimate

Space Science Reviews **60:** 503–530, 1992.
© 1992 *Kluwer Academic Publishers. Printed in Belgium.*

deposition in the Jupiter auroral zone. Spectra from the International Ultraviolet Explorer and rocket-borne spectrometers, along with data from the UV channel of the Voyager Photopolarimeter have revealed photochemical products of CH_4 and auroral zone darkening phenomena that will be addressed by emission and absorption spectroscopy in the 115–340 nm wavelength region of the UVS. The new, longer wavelength region available on Galileo will provide the opportunity to study the micro- and macroscopic properties of the cloud particles in the atmosphere of Jupiter. Satellite surface scattering properties will be explored in concert with the Near Infrared Mapping Spectrometer (NIMS) investigation to understand the evolutionary history of these surfaces.

2. Scientific Objectives

2.1. Interplanetary Medium

The interplanetary medium is supplied with atoms of hydrogen and helium by the interstellar wind. Both species are detectable by the UVS through their resonance scattering of solar photons at 121.6 and 58.4 nm (Thomas, 1978). Gravitational focussing by the Sun produces a cone of enhanced helium abundance downwind of from the Sun; the density and shape of this cone reflects the velocity distribution of atoms in the ISW. In contrast, a cavity in the hydrogen medium is created by charge exchange with solar wind protons, and the atoms of hydrogen experience a repulsion due to radiation pressure that is comparable to solar gravity. The size and shape of the cavity depends on variables such as the solar wind, Lα and EUV fluxes (all of which vary with solar longitude and latitude), as well as the characteristics of the ISW itself. Processes occurring at the heliopause may also affect the cavity. By carrying out a systematic program of H and He measurements over the course of the mission, UVS will improve our knowledge of the ISW and of the processes that affect its passage through the solar system. Of interest early in the mission will be the search for evidence of an inner-solar-system source of hydrogen, perhaps from subvisual comets. Observations by UVS and EUV should be a more sensitive search than those of the Voyager UVS, from which Hall and Shemansky (1988) have derived an upper limit to the possible Lα signal.

2.2. Venus

Very little is known about the EUV spectrum of Venus, while the UV spectrum has been extensively studied. EUV measurements will tell us about the ratio of O^+ to O and H. The geometry of the Galileo flyby will permit pole-to-pole and dawn-to-dusk measurements of the abundance of SO_2 in the cloud-top region, and of the abundances of O and CO in the thermosphere. The latter quantities are determined by the balance between global-scale solar-driven thermospheric wind systems and vertical transport induced by the dissipation of tides and gravity waves. The wind systems carry atoms of oxygen and nitrogen to the night side, where they undergo chemiluminescent recombination to form O_2 and NO (Lawrence *et al.*, 1977; Stewart and Barth, 1979). The broad

wavelength coverage of UVS will allow the simultaneous measurement of the resulting NO and O_2 emissions, whose distribution over the night side reflects the high- and low-altitude components of these winds. The altitudes of the emitting layers are also of dynamical interest. In the far UV, the altitude of emissions from O will constrain the energy of auroral electrons that presumably derive either from the daytime topside ionosphere or from the solar wind itself.

2.3. Earth and Moon

Although the UV and even the EUV emissions from the Earth have been extensively studied, the two Galileo flybys offer opportunities to address unanswered questions. As on Venus the post-encounter passage near the subsolar point at long range allows the near-simultaneous measurement of pole-to-pole and dawn-to-dusk variations in the UV airglow and in reflected sunlight. From the former we can investigate the global O/N_2 ratio through their respective UV emissions, while from the latter we can investigate the distribution of ozone. It is also of interest to establish the Earth's UV albedo in the Schumann–Runge band region near and below 200 nm; the absorption of solar photons in this spectral range produces photodissociation in the mesosphere and is an important energy source for the photochemistry of that region.

A search for a tenuous lunar atmosphere using the resonance emissions of H, O, and OH will address the question of the rate of bombardment of the Moon by small bodies, and of the fate of solar wind protons that strike the surface. Previous searches of this kind have had negative results (Fastie *et al.*, 1973), but the possibility of episodic events remains. The flybys also allow the Earth–Moon system to be mapped, and these data will also contain an image of the hydrogen geocorona from a unique sunward vantage point.

2.4. Asteroids

The UVS will measure the albedo of the asteroids Gaspra and Ida during flyby. Spatial resolution on the bodies' surfaces will not be possible, but their scattering properties as a function of phase angle will be measured, and the presence of absorption features at wavelengths longer than 200 nm will be determined. At these and at shorter wavelengths (down to Lα) the asteroid's albedo may be directly compared to that of the Moon measured during the two Earth encounters.

2.5. Jovian Atmosphere

2.5.1. *Clouds and Hazes*

The Galileo orbiting mission offers the opportunity to observe Jupiter's clouds and hazes repeatedly over a wide range of phase angle and wavelength; the imaging and mapping capabilities of the optical instruments will allow these studies to be made on individual cloud features as well as on planetary-scale features. Because its ability to examine small scattering angles is restricted by solar protection considerations, the contribution of UVS will be to determine the imaginary parts of the aerosols' refractive

indices by obtaining the single-scattering albedo from photometric measurements. It will sample the lower end of the aerosol size distribution due to its sensitivity down to 200 nm. The distribution of aerosols with altitude will be measured in the stratosphere by measuring limb radiance profiles and in the troposphere by making nadir-to-limb scans.

Regarding time variations, optical observations from Earth, Earth orbit, and flyby missions indicate great changes on many spatial and time scales (Beebe *et al.*, 1989). No clear seasonal patterns have been identified, but changes in the color, structure, and albedo of belts and zones and of smaller features have been seen on timescales of years and sometimes months. Galileo's tour designs favor observations of the morning hemisphere, and offer the opportunity for detailed spectroscopic and photometric studies at timescales ranging from days to the duration of the mission (about two years, less than a complete Jovian season).

2.5.2. *Stratospheric Composition and Chemistry*

Jupiter has a reducing atmosphere whose photochemistry is dominated by the photolysis of methane (Strobel, 1975). Its derivatives, C_2H_6, C_2H_4, and C_2H_2 are removed by vertical transport. C_2H_2 (acetylene) initiates a reaction chain leading to aerosol formation, and these aerosols are also removed by transport. Methane and ethane (C_2H_6) are detectable in UV reflectance by broad absorption continua below 160 nm, and C_2H_4 and C_2H_2 have characteristic strong absorption bands in the same region. UVS will use reflectance spectroscopy during disc and limb scans to compile an inventory of these hydrocarbons as a function of location and altitude; the models of photochemistry, vertical transport, and aerosol formation can be tested against these data, and horizontal variations will indicate the zonal and meridional variations in vertical transport processes. UVS limb scans will yield stratospheric temperatures through the scale height of the signal from Rayleigh scattered sunlight. These scale heights are a factor in the retrieval of vertical transport parameters, and the temperatures may affect the photochemistry.

Stratospheric temperatures show considerable variations (Beebe *et al.*, 1989). At the time of the Voyager flybys, which occurred near northern autumnal equinox, stratospheric temperature contrasts of order 10 K were noted between the northern and southern hemispheres. Galileo will observe Jupiter near northern vernal equinox, and a reversal of the contrast, which has been attributed to the greater summer insolation in the northern summer due to proximity to perihelion (Caldwell *et al.*, 1979), will be looked for. The Voyagers also noticed a 2 K equatorial warming over the 4 months between the flybys (Geirasch *et al.*, 1986) such variations will be readily studied by Galileo, whose mission will consist of orbits with periods between 1 and 4 months.

2.6. THERMOSPHERE

The thermosphere of Jupiter is characterized by unexpectedly high temperatures (of order 1100 K in the upper thermosphere) and by unexpectedly bright UV emissions from molecular hydrogen. Lα emission from H shows an equatorial bulge that sometimes

extends across the morning terminator. None of these phenomena have been totally explained. Diffuse fluxes of soft electrons have been proposed (the 'electroglow' concept) but the existence, the energy source, and the need for such electrons all remain controversial (Clarke *et al.*, 1989a). The ionospheric electron density profiles measured by radio occultation techniques from the Pioneer and Voyager spacecraft are also poorly understood (Eshleman *et al.*, 1979). Emission, heating, and ionization are slightly linked processes, and a careful study of spectral, horizontal, vertical, and diurnal and other time variations is an important objective for the Galileo UVS and EUV experiments.

2.7. Aurora

The Jovian aurora has been observed at X-ray, EUV, UV, and IR wavelengths (Clarke *et al.*, 1989a). There is considerable uncertainty about the nature of the primaries, and indeed there may be several different types of aurora, produced by the precipitation of energetic electrons, protons, and heavy ions (oxygen and sulfur from the Io torus). In the UV the dominant emissions are H Lα and the Werner and Lyman bands of H_2. The spectrum of the H_2 bands clearly show the effects of absorption by acetylene, indicating that the primaries penetrate at least as deep as the homopause (Gladstone and Skinner, 1989). The Lα emission shows none of the Doppler-shifted component to be expected from precipitating protons or hydrogen atoms (Clarke *et al.*, 1989b). The X-rays may be bremsstrahlung or emissions from torus ions (Metzger *et al.*, 1983). The IR emissions are attributed to CH_4, C_2H_2, and other trace gases; they indicate enhanced temperatures in auroral 'hot spots'. These hot spots are located on the traditional 'auroral zone' lying at the feet of magnetotail field lines, whereas the UV and EUV emissions are observed at the feet of lines intersecting the Io torus. In both cases the emissions are preferentially seen near 180° System III longitude. In the southern hemisphere, there is a broader clumping of UV emissions around 0° longitude.

Galileo's mostly equatorial orbits mean that the aurora will be observed near the northern or southern limbs, allowing excellent longitudinal resolution at the cost of lesser latitude resolution. The spectral effects of atmospheric absorption will be enhanced. Jupiter's rapid rotation will facilitate the determination of longitudinal dependences of the emissions on each orbit. The possibility of correlations between the aurora and conditions in the Io torus will be explored.

2.8. Satellites

While close-range observations of Io and Europa will be prevented by the radiation environment, the outer two Galilean satellites will be visited many times in close (from a few hundred km up) encounters. Io's surface is dominated by the effects of its vulcanism, and it appears to possess an atmosphere of sulfur dioxide. Europa has a young, icy, frequently resurfaced exterior, marked by light and dark lineaments. Callisto's surface is dark and heavily cratered with very little evidence of volcanic activity. Ganymede has a surface part of which resembles Callisto's and part of which is light-colored and extensively marked by extensional events. The entire surface shows systems of grooves.

The Galileo UVS will measure and map the UV albedos of these moons. The measurements will be compared with those of the Moon and of the asteroids Gaspra and Ida. The rich variety of surface terrain and materials will greatly expand our knowledge of the UV scattering properties of satellite surfaces. The UVS will also look for evidence of tenuous and possibly sporadic atmospheres that might be produced by sublimation, sputtering by co-rotating plasma, or even eruptive events.

2.9. Io Torus

The torus of Io is produced by the ejection of material from Io, its subsequent ionization mostly by charged particle bombardment, and the pickup of the resultant ions by the rotating magnetic field of Jupiter (Strobel, 1989). Prior to ionization, the neutral material leaving Io forms a 'neutral cloud' under the influences of Jovian gravity and, for some species, radiation pressure. Conditions in the torus thus reflect the surface and atmospheric composition of Io and the nature and efficiency of the escape and ionization processes, as well as the complex interactions of the ionized material with the magnetic and gravitational fields of Jupiter and with the rest of the magnetosphere. Information on these materials and processes can be gained by measuring the abundance and distribution of the neutral and ionized species. The EUV instrument will perform this task for the ionized states of sulfur and oxygen, whose origin is ultimately the venting of sulfur dioxide from Ionian volcanoes. The UV instrument will measure neutral sulfur and oxygen. The relative abundances of the neutral and ionized states of these gases reflect local plasma density and especially the electron temperature. The EUV will observe the torus on inbound orbital legs, for a period equal to several Jovian rotations and comparable to a revolution of Io; thus the data will reveal many dynamical aspects of the torus in addition to its composition. Spatial resolution will be best at the sunward ansa which will be viewed from about 20 R_J on the early orbits. The absolute brightness of the emissions, especially those from ionized sulfur and oxygen in the EUV, are of great importance because the emissions are a major cooling process for the heated torus plasma, whose energy balance is not fully understood (Strobel, 1989). The range of variability in torus conditions with time is also inadequately explored; the combination of an approximately two-year timebase and high spatial resolution offered by Galileo will be invaluable.

2.10. Magnetosphere

There are many processes in the exosphere of Jupiter, on the constantly irradiated satellites, in the Io torus, and in the magnetosphere in general, that might provide sources of neutral atoms in the magnetosphere. We might expect to find hydrogen and even OH in addition to oxygen and sulfur. The UV instrument will search for such material at times when the radiation noise in the instrument is at a minimum.

2.11. Joint investigations

Collaborative studies are planned with the fields and particles investigators. Our goal is to improve our understanding of the transportation of sulfur and oxygen ions from

the Io plasma torus to their ultimate precipitation in the Jupiter auroral region. The *in-situ* particle measurements will describe the ion and electron populations in the Io torus. Ultraviolet emissions from torus ions, and possibly neutrals, in the 55–430 μm range provide temperature, radiative energy loss, and compositional information that will help constrain physical conditions of the torus. *In-situ* measurements of the torus can be made on only the two passages of the spacecraft through the torus region. Ultraviolet data can obtain torus data on every orbit of Jupiter extending and measuring variability over the full length of the mission. Ultraviolet measurements of auroral emissions from atomic and molecular hydrogen will depend on the knowledge of the quantity and energy distribution of electrons impacting the upper atmosphere of Jupiter.

Joint investigations with the Photopolarimeter Radiometer experiment will help define the particulate properties of the Jupiter atmosphere. Ultraviolet brightness measurements at 1.3 μm resolution in the 200–320 μm wavelength region will complement visible and near-infrared polarimetric measurements. Measurements of brightness as a function of emission, incidence and phase angle will define the effective particle phase function over a broad wavelength range, providing constraints on cloud particle size, shape, and composition. Complementary ultraviolet spectrometer and photopolarimeter observations will provide information about the spatial extent and altitude distributions of these clouds.

Properties of the satellite surfaces will be measured in cooperation with the Near Infrared Mapping Spectrometer, the Photopolarimeter Radiometer, and the Solid State Imaging Instrument. The Ultraviolet and Infrared spectrometers provide extended wavelength coverage from 55 μm up to nearly 5 μm. Scattering properties as well as ultraviolet absorbers, e.g., sulfur dioxide, will be measured to add leverage to our understanding of the Galilean satellites.

3. UVS Instrument Description

The Galileo Ultraviolet Spectrometer (UVS) consists of a Cassegrain telescope and a Ebert–Fastie scanning spectrometer (see Figures 1 and 2 and Table I). Spectral scanning is accomplished using a fully programmable diffraction grating drive. Three separate photomultiplier detectors, located in the exit focal plane of the spectrometer, are used to cover the entire ultraviolet-near-visible spectrum from 113 to 432 nm. Spectral scanning, instrument command and control, data formatting, and spacecraft interface are all controlled using an RCA Sandia CDP 1802 microprocessor within the instrument.

3.1. Telescope

The optical design for the UVS telescope is a Dall–Kirkham configuration (elliptical primary mirror and spherical secondary mirror) with an effective focal length of 250 mm and a focal ratio of $f/5$. In order to measure accurate limb profiles, the telescope has been equipped with an external sunshade and an extensive baffle system for rejection of off-axis scattered light. The field of view is wavelength-dependent, being limited by

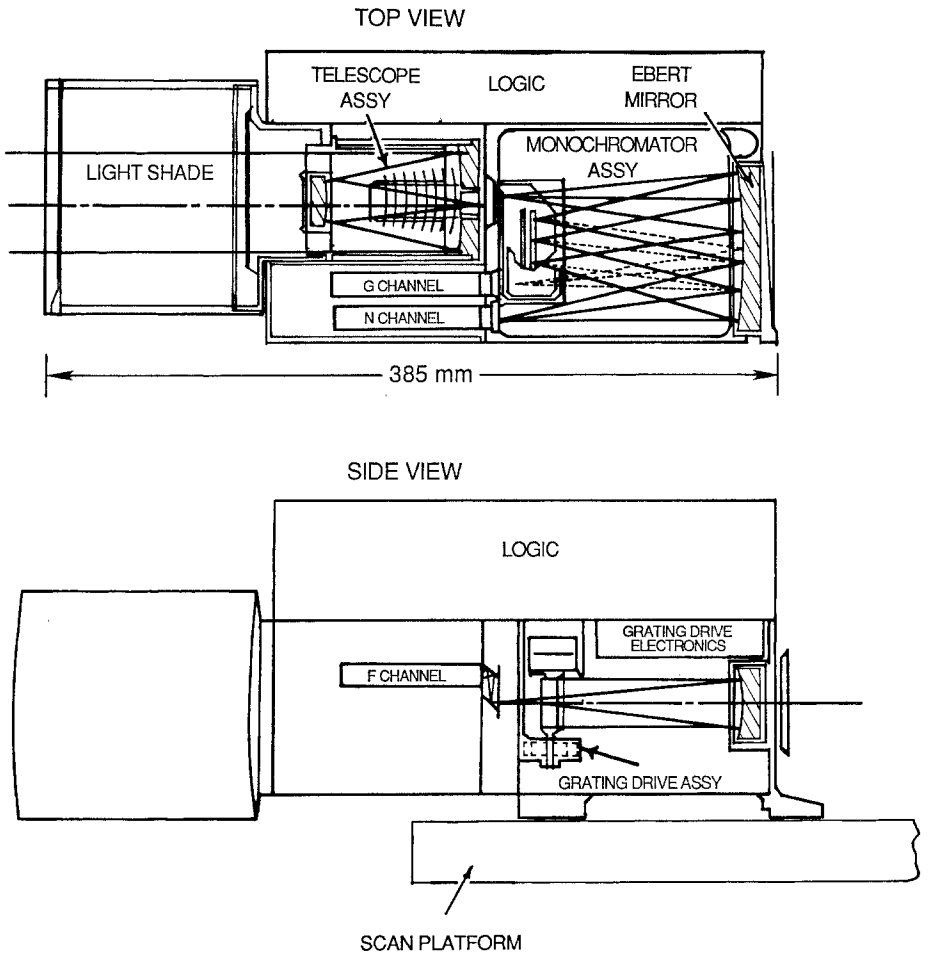

Fig. 1. UVS Mechanical Optical Configuration. The top panel is a view of the UVS looking down onto the spacecraft scan platform. Solid lines superimposed on the instrument figure show the light path through the instrument to the near-ultraviolet-visible detector (*N* channel). In order to reach the far-ultraviolet detector (*G* channel) light travels on a different path from the grating to the detector assembly as shown by the dotted line. The field of view of the telescope is 0.1° in this plane. The bottom panel shows a side view of the instrument mounted on the scan platform. The solid line represents the light path from the grating to the near-ultraviolet detector (*F* channel). In this plane the telescope fields of view are 1° for the *G* and *N* detectors and 0.4° for the *F* detector.

the spectrometer entrance slit to 1° × 0.1° for two of the detectors (113 to 192 nm) and (282 to 432 nm) and by one of the spectrometer exit slits to 0.4° × 0.1° for the third detector (162 to 323 nm).

A bright object sensor (limb sensor) with a 1.5° FWHM field of view located below the telescope sunshade structure is used to protect the long wavelength detector during atmospheric limb observations.

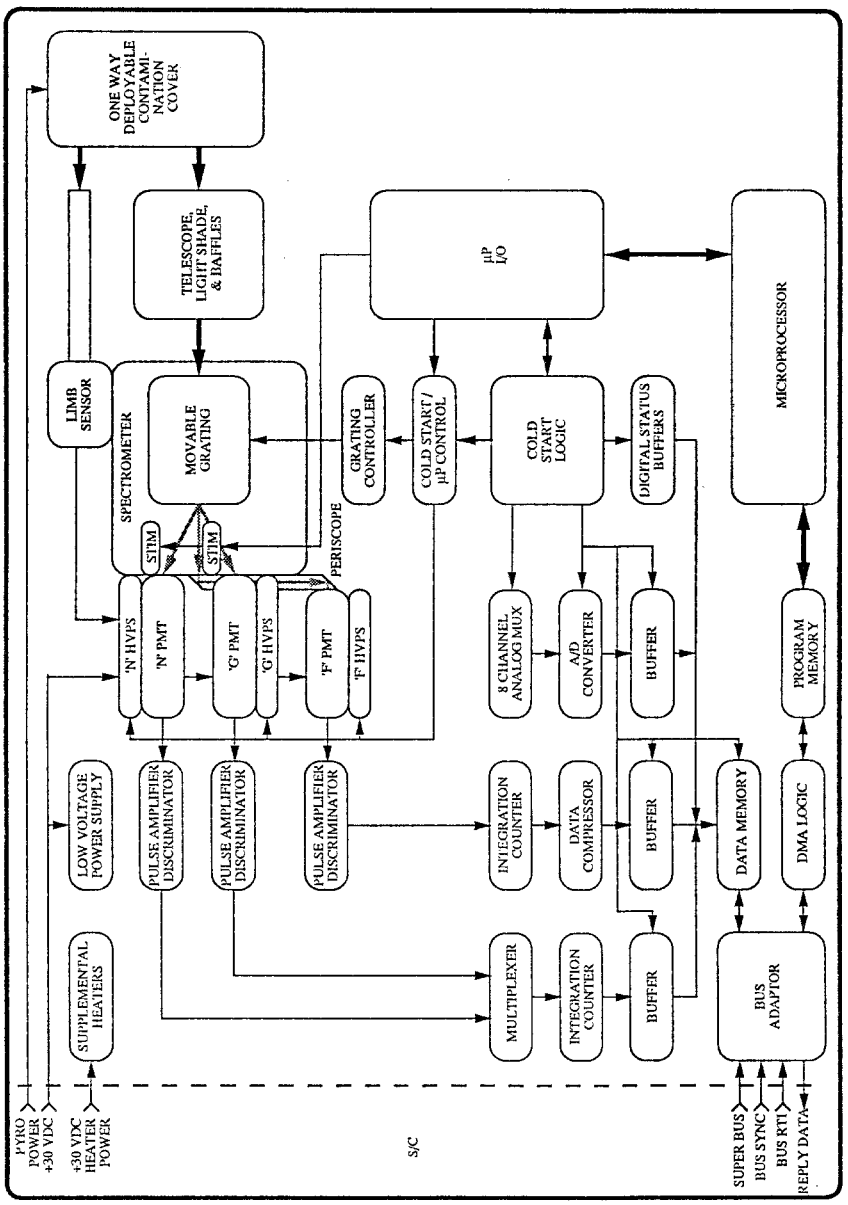

Fig. 2. UVS functional block diagram.

TABLE I

Summary of UVS characteristics

Telescope	
Focal length	250 mm
Focal ratio	*f*/5
Aperture	50.3 mm × 52.8 mm
Unobscured area	13.89 cm^2
Spectrometer	
Focal length	125 mm
Grating	
Ruling	2400 lines per mm
Blaze angle	16.75 deg
Detectors	
G channel	EMR 510G-09 CsI photocathode
F channel	EMR 510F-06 CsTe photocathode
N channel	EMR 510N-06 KCsSB photocathode
Nominal wavelength range	
G channel	113.3–192.1 nm 2nd order
F channel	162.0–323.1 nm 1st order
N channel	282.0–432.0 nm 1st order
Nominal resolution	
G channel	0.67 nm
F channel	1.36 nm
N channel	1.27 nm
Field of view	
G and *N* channels	0.1 × 1 deg
F channel	0.1 × 0.4 deg
Exit slit solid angle	
G and *N* channels	3.05×10^{-5} steradians
F channel	1.20×10^{-5} steradians
Instrument	
Mass	5.2 kg
Power	2.4 W

3.2. SPECTROMETER

The spectrometer is a standard, 125-mm-focal-length, Ebert–Fastie design which uses a single spherical mirror as both collimator and camera and a plane diffraction grating. A ruling density of 2400 grooves per mm provides a first-order dispersion of 2.9 nm per mm and an average spectral resolution of 200 for a 0.43-mm-wide entrance slit (0.1° telescope field of view).

Three EMR Photoelectric Corp. 510 photomultiplier tubes, located behind three separate exit slits in the focal plane of the spectrometer record the spectrum in three overlapping wavelength ranges. Each detector has its own high voltage power supply and pulse counting electronics, allowing for independent operation. Photocathodes and windows for the detectors were chosen to optimize measurements in narrow spectral ranges. The far-ultraviolet detector (*G* channel) is equipped with a MgF_2 window and a cesium iodide photocathode resulting in a solar blind detector with high sensitivity in the wavelength range 113 to 192 nm. The middle-ultraviolet detector (*F* channel) is

equipped with a quartz window to block radiation below 160 nm and a cesium telluride photocathode to suppress its response to radiation from wavelengths longer than 350 nm. The near-ultraviolet-visible detector (N channel) is equipped with a quartz window and a bi-alkali photocathode and is sensitive to radiation in the wavelength range 160 to 450 nm.

All three detectors are mounted in a single mechanical housing along with their high voltage power supplies and pulse-amplifier-discriminators. The G and N photomultipliers are located directly behind their respective exit slits in the spectrometer housing. Volume constraints require that the F photomultiplier be mounted above the slit plane and light is directed to it by a small two mirror periscope located behind the F channel exit slit (see Figure 1).

Spectral scanning is accomplished by rotating the diffraction grating. The UVS grating drive uses a moire fringe pattern, generated by overlaying two radially etched transmission gratings, to control the angular position of the grating. One of the transmission gratings is fixed, and the other rotates with the diffraction grating housing. The fringe cycles are detected using two solid state detector-emitter pairs, located relative to the radial gratings so that one pair detects a sine modulation and the other detects a cosine modulation. The sine and cosine modulated signals are combined with a 10 kHz reference signal $\sin(\omega t)$ to produce a Control Phase Signal (CPS) $\sin(\omega t + a)$ (see Figure 3). In order to rotate the grating, the control electronics generates a second

GRATING DRIVE FUNCTIONAL BLOCK DIAGRAM

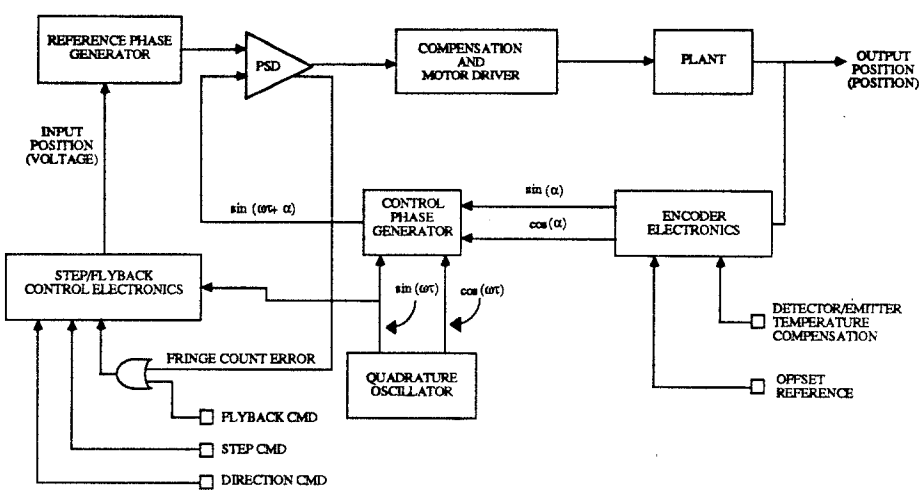

Fig. 3. UVS grating drive functional block diagram.

10 kHz Reference Phase Signal (RPS). The phase of the RPS is shifted in 64 equal steps through 2π and is used as a step input to grating drive control system. After the phase of the RPS is incremented, it is compared to the CPS using the Phase Sensitive Detector

(PSD) electronics. The PSD electronics produce an error signal which is proportional to the phase difference between the RPS and the CPS. This error signal is applied to the motor drive to null the difference in the two signals resulting in a step rotation of the diffraction grating. Since the grating drive is an incremental, rather than absolute, encoding system, the PSD electronics must also generate a fringe count error signal to insure that the system does not control on an adjacent fringe.

The transmission gratings have a ruling of 1500 lines per 360° rotation resulting in a single cycle of 0.024° and a single phase increment step size of 0.00375°. Each grating step for the UVS is a sum of six phase increment steps or 0.0225°. Thus a grating step results in a 0.1-mm displacement of the spectrum in the spectrometer focal plane so that the spectrum is sampled on the average of 4 times per spectral resolution element.

3.3. Microprocessor and bus adaptor

The UVS uses an RCA 1802 CMOS microprocessor for command parsing, spacecraft time recognition and synchronization, and instrument control. In addition, the UVS design incorporates additional electronics called the Cold Start Logic (CSL) that places it into a cyclical $F-G$ scan mode (see below) until microprocessor control is initiated by spacecraft command.

The microprocessor receives commands and spacecraft timing information via the Bus Adaptor and associated Direct Memory Access (DMA) logic.

The Bus Adaptor serves as the bi-directional interface between the Galileo spacecraft and the UVS. Its circuitry serves to isolate the UVS electrically from the spacecraft and to allow for 8-bit information flow to and from the UVS.

3.4. Modes of operation

Modes of operation for the UVS are designed to be compatible with a data rate of 1 kbits per second and with the basic spacecraft major frame time period of $60\frac{2}{3}$ s. For the UVS operation each major frame is subdivided into 14 UVS 'science frames' each of $4\frac{1}{3}$ s duration.

The basic data frame for the spectrometer is a detector counting integration time (accumulation) followed by a single grating step. Each data frame is fixed in length to 7.6 ms with 1.6 ms allocated to step the grating. Output pulses from the G and N detectors are accumulated in an 8-bit counter and then routed to a circular output buffer. Output pulses from the F detector are accumulated in a 16-bit counter and then log compressed to 8 bits before routing to the circular output buffer. In order to minimize spectral smearing caused by step and settling time when the grating drive mechanism changes positions, only one step is allowed between successive data frames. Data from a single UVS science frame consists of 18 8-bit words of engineering data and 528 words of science data which are acquired in a 4-s period. The final $\frac{1}{3}$ s of each science frame is used for large motions of the grating drive; either fly-back to the zero-step position or step to a different wavelength to initiate a mini-scan (see below).

3.5. Scan modes

The UVS software supports two distinct operations modes: (1) 'Scan' mode, and (2) 'Fixed Wavelength Mini-Scan' mode.

When the UVS is commanded into any of the Scan modes, the instrument starts integrating at one end of the spectrum for a single detector, and steps the grating (one step per 7.6 ms) to the other end of the detector's spectral range, using 528 steps over a 4-s science frame.

In any given Scan mode, either one or two spectral regions can be covered. If only one region is desired then the microprocessor steps the grating up the wavelength scale during even-numbered Science Frames and down on odd-numbered Science Frames. If two regions are selected, for example the N and G channels, then the microprocessor scans up the N channel on even-numbered Science Frames and down the G channel on odd-numbered Science Frames. Any single or combination of two detectors can be used for a total of six scan modes.

3.6. Fixed-wavelength mini-scan modes

These modes were designed to perform detailed studies of various features in the spectrum. For this set of modes, only one detector may be selected for investigation per command. Within the spectral range for the selected detector, from one to four separate spectral regions can be scanned in a sawtooth pattern. The microprocessor will position the grating drive to the bottom of the first spectral region, and will then perform the mini-scan sawtooth motion for a programmable number of steps up and down for 4 s. During the $\frac{1}{3}$-s dead time the grating will be positioned at the bottom of the next feature. This feature will then be mini-scanned for 4 s. The process will continue in a 1–2–3–4–4–3–2–1 pattern until receipt of a new command (note that if only two features are commanded, the sequence is 1–2–2–1, etc.).

3.7. Calibration and laboratory performance

The instrument parameters which most directly influence the proper evaluation of science data returned by the UVS are: instrument absolute sensitivity, spectrometer wavelength scale and band pass, telescope scattered-light rejection, and instrument polarization. For an extended source the UVS count rate can be expressed as

$$C = I\omega A Q_e \tag{1}$$

where I is the source radiance, ω is the angular field of view of the spectrometer exit slit, A is the telescope collecting area, and Q_e is the instrument absolute efficiency.

If I is measured in units of 10^6 photons $\mathrm{cm}^{-2}/4\pi$ steradians s^{-1}, then C is expressed in counts per Rayleigh.

Instrument absolute sensitivity was measured using source standards which are traceable to the National Institute for Standards and Technology (NIST). For wavelengths greater than 200 nm an NIST deuterium lamp (200–350 nm) and an Optronics Laboratories Inc. FEL tungsten-halogen lamp (250–432 nm) were used to illuminate a barium sulfate scattering screen. Because the screen closely approximates a Lambertian

radiator, its radiance (photons per second per unit area per unit solid angle) could be calculated directly from the lamp flux (photons per unit area per second) impinging on it. Observation of the scattering screen resulted in a direct measure of the instrument response to an extended source which fills the telescope field of view.

For wavelengths in the range 115–310 nm the instrument sensitivity was measured in the University of Colorado's Laboratory for Atmospheric and Space Physics (LASP) vacuum calibration facility (McClintock *et al.*, 1982) using detector standards traceable to the NIST. The instrument was illuminated with a nearly monochromatic collimated beam of photons from a laboratory spectrometer-telescope. The flux of photons impinging on the instrument aperture was measured by scanning the input beam with a pulse-counting photomultiplier tube which was calibrated using an NIST standard photodiode. The ratio of instrument counts per second to input beam flux measured the product of the UVS telescope area and the instrument absolute quantum efficiency, AQ_e. Because the input beam is highly collimated, it was necessary to scan the 'point' object along the 1° UVS entrance slit and fold that spatial response into the absolute sensitivity measurement made with the point source at slit center to measure the effective value of ω. Two sets of measurements were averaged: one taken with the UVS grating and the laboratory spectrometer grating grooves parallel, and one with the grooves perpendicular in order to avoid polarization-induced changes in efficiency.

Independently from the source and detector standards, relative sensitivity measurements for 115–220 nm were made using an electron lamp (Ajello *et al.*, 1988). Using both H_2 and N_2 as source gases allowed the relative shape of the lamp spectrum to be calculated to about 10%. Figures 4 and 5 show sample spectra of H_2 and N_2 taken with the UVS G and F channels, respectively.

Figure 6 shows results synthesized from all three calibration techniques. The ordinate is the sensitivity C in counts s^{-1} per Rayleigh for a monochromatic source. If the source radiance is expressed in Rayleighs per nanometer, then the results must be multiplied by 1.27, 1.36 and by 0.67 for the N, F, and G channels, respectively. Estimated accuracies in the absolute calibrations are 15% for the F and N channels and 20% for the G channel.

The pulse-counting electronics for the detectors have a dead time which inhibits counting of photo-events. Dead-time corrections were measured for each detector using a stable lamp and a set of precision pinholes. Within the accuracy of the measurements the number of true counts per second is related to the number of observed counts per second and can be calculated from the relation

$$Ct = \frac{C_0}{1 - C_0\tau}$$

where $\tau = 6.25 \times 10^{-7}$ s. The relation is valid within 10% for $C_0 \leq 5.2 \times 10^5$ counts s^{-1}.

Spectrometer wavelength scale and band pass were measured by observing a scattering screen illuminated by mercury and platinum emission line sources. Wavelengths determined by a best fit to the grating equation agree with published values to within

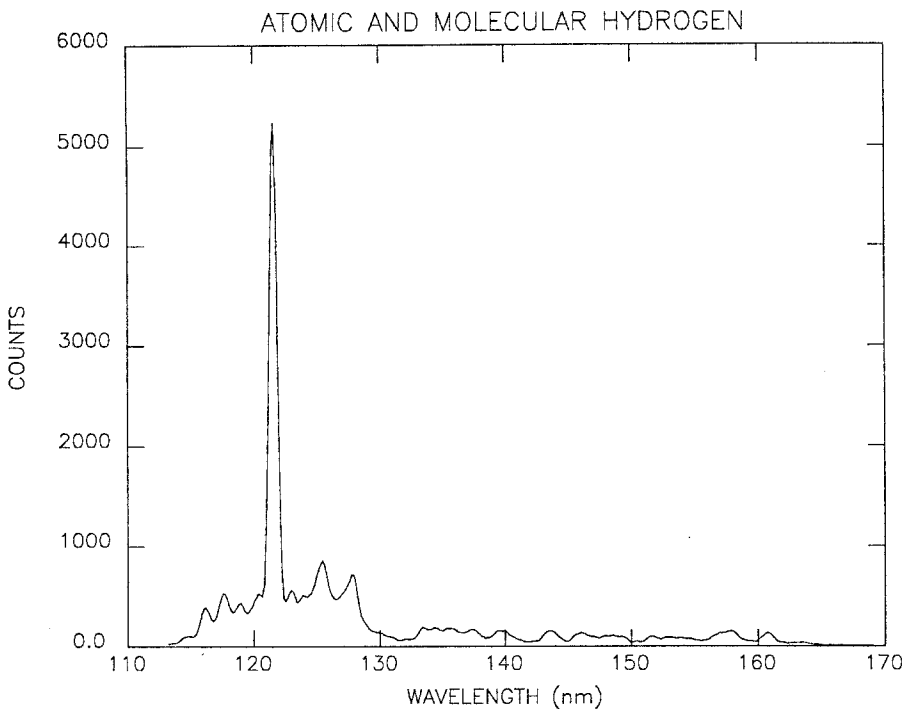

Fig. 4. An electron impact spectrum of hydrogen obtained with the UVS *G* channel. The prominent emission features are the Lα line of atomic hydrogen at 126 nm and the Lyman and Werner band systems of molecular hydrogen.

± 0.2 nm. The line shape is well fit by a Gaussian profile with an average FWHM of 4.5 grating steps. Measurements of grating scatter show no ghosts greater than 0.01% of the parent line within 50 nm of parent line center.

The amount of false signal caused by long wavelength radiation which scatters through the exit slits from surfaces within the spectrometer housing was measured for the *F* and *N* detectors using a tungsten-halogen lamp and a series of long wavelength pass spectral filters. These measurements were connected to an equivalent source radiance using the telescope collecting area and entrance slit field of view. For the *F* channel the scattered light false signal varies from 6.7×10^{-7} counts s^{-1} Rayleigh^{-1} at 350 nm to 6.7×10^{-9} counts s^{-1} Rayleigh^{-1} at 400 nm to 1.3×10^{-9} counts s^{-1} Rayleigh^{-1} at 450 nm. For the *N* channel the scattered light false signal varies from 3.5×10^{-5} counts s^{-1} Rayleigh^{-1} at 500 nm to 2.3×10^{-8} counts s^{-1} Rayleigh^{-1} at 750 nm.

The *G* channel operates in second order from 113 to 192 nm and second-order radiation for 226 to 394 nm which is imaged directly onto that exit slit and rejected by the very low response of the CsI photo cathode to those wavelengths. For 253.7 nm the

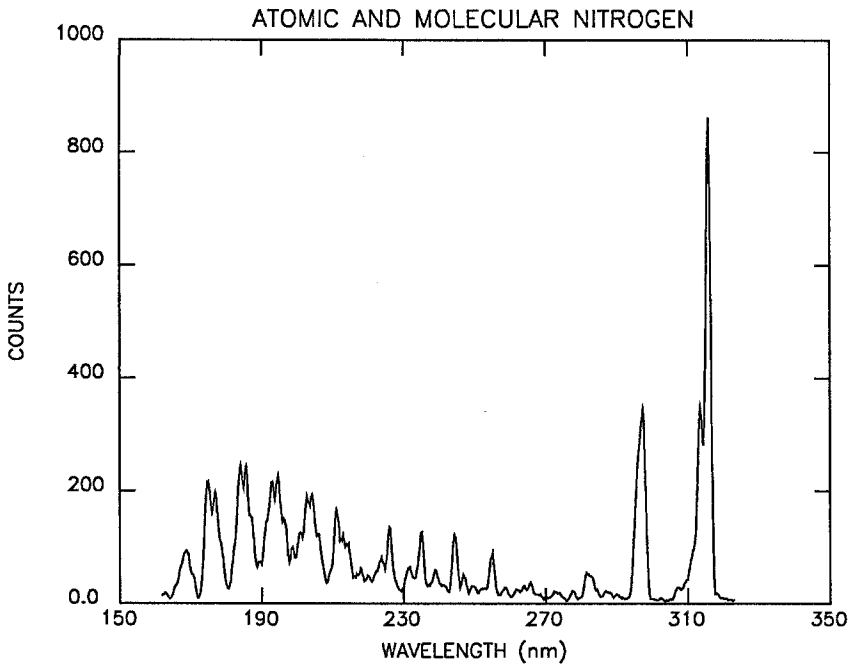

Fig. 5. An electron impact spectrum of nitrogen obtained with the UVS *F* channel. The prominent features are the Lyman–Birge–Hopfield bands and the second positive system of molecular nitrogen at 160–255 nm and 296–316 nm, respectively.

measured response is less than 8.5×10^{-7} counts Rayleigh^{-1} s^{-1}. For 365 nm the calculated response is less than 4.2×10^{-9} counts Rayleigh^{-1} s^{-1}.

Figure 7 is a plot of the normalized off-axis response of the telescope to a point source made as its image was scanned across the narrow dimension of the spectrometer entrance slit. Very close to the optic axis the shape of the scattering curve is dominated by the micro roughness of the telescope mirror surfaces. At larger angles, the curve is dominated by the telescope baffle system and sun shade.

Sensitivity to polarization in the UVS is due almost entirely to the diffraction grating. Figure 8 shows the polarization response of the UVS plotted as the ratio of $(I_{\text{para}} - I_{\text{perp}})/(I_{\text{para}} + I_{\text{perp}})$ where I_{para} (I_{perp}) are the instrument response to light polarized with its electric vector parallel (perpendicular) to the grating grooves.

4. EUVS Instrument Description

The Galileo EUVS channel is an objective grating spectrograph covering the wavelength range of 54–128 nm in 128 contiguous intervals of 0.59 nm. Figure 9 is an optical diagram. The Galileo EUVS channel consists of the flight spare Voyager Ultraviolet Spectrograph (Broadfoot *et al.*, 1977) and an electrical interface to adapt it to the Galileo command and data bus (Figure 10). We have modified the instrument from its Voyager

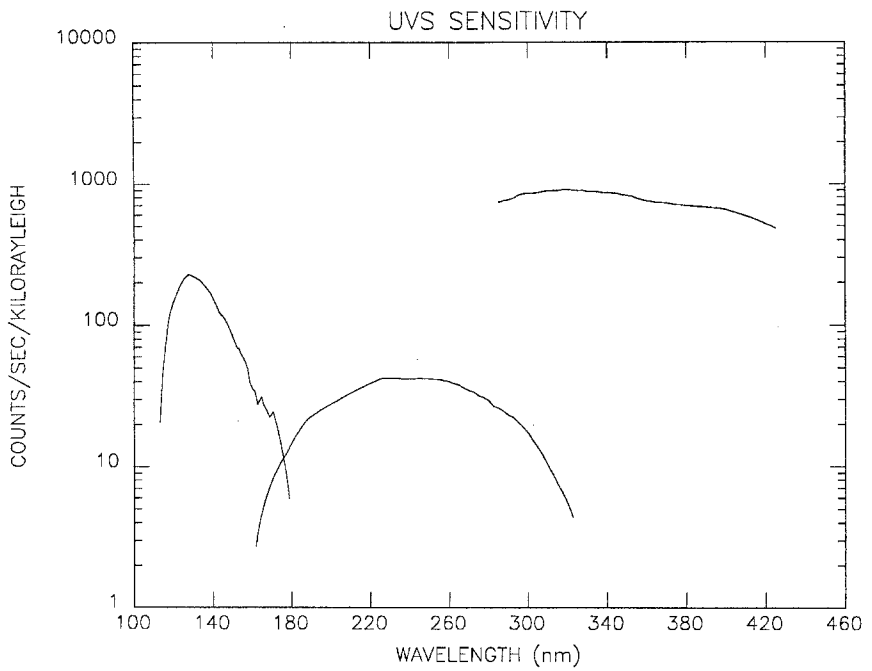

Fig. 6. Composite UVS sensitivity in counts per second per Rayleigh for a monochromatic emission line which fills the field of view. When the source radiance is expressed in Rayleighs per nanometer, the sensitivities must be multiplied by 1.3 for the *F* and *N* channels and by 0.67 for the *G* channel. Estimated accuracies in the absolute calibrations are 15% for the *F* and *N* channels and 20% for the *G* channel.

configuration to increase by 70% its field of view in the dispersion direction, and we have changed the grating to increase the dispersion by 40%. The characteristics of the EUVS channel are summarized in Table II.

4.1. Optical configuration

An objective grating spectrograph is commonly used for observations of point sources. An open, or reflective, optical system is required for wavelengths less than 104 nm, the shortest wavelength transmitted by a refractive material. The low reflective efficiencies at these wavelengths, except at grazing incidence, limit an instrument intended for the study of weak emissions to a single reflection. We have adapted the objective grating design to observe extended sources by restricting the field of view in the dispersion direction. The field is restricted by a series of mechanical stops that we call the 'collimator' because it controls the angle at which the grating is illuminated, as does a traditional optical collimator. The combination of grating and collimator has the properties described by Wadsworth in 1896 and Beutler in 1945 (Hale and Wadsworth, 1896; Beutler, 1945). The collimator was designed to induce negligible Fresnel diffraction, but the mechanical structure causes a loss of about $\frac{2}{3}$ in effective aperture, and scattering from the edges of the aperture plates complicates the analysis of the spectrum to some

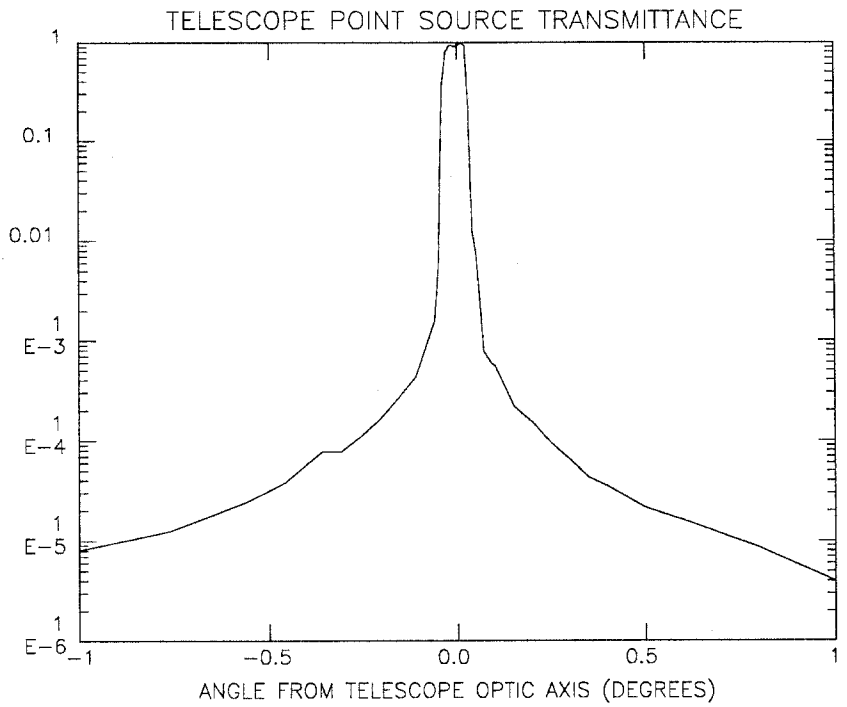

Fig. 7. Normalized off-axis response for the UVS telescope. Beyond 1° off axis the response continues to decrease by a factor of 2.1 per degree ($R = 10^{-6}$ at 4° off axis). No measurements were made beyond 4°. The rate of decline is expected to decrease beyond 15°, which is the largest angle at which light is directly incident on the telescope primary mirror.

TABLE II

Summary of EUVS characteristics

Location	Spinning section
Field of view	
Orientation	Perpendicular to spin axis
	long axis of slit parallel to spin axis
Size	0.17 deg (dispersion direction)
	0.86 deg (cross-dispersion direction)
Optical configuration	Objective grating spectrograph with mechanical grille collimator
Detector	Microchannel plates and self-scanned anode array
	128 channels scanned at 3125 Hz
Grating	Holographically fabricated
	842 lines/mm
	iridium coated
Dispersion	0.59 nm channel^{-1}
Wavelength range	54–128 nm
Focal length	200 mm
Aperture	40 × 60 mm
Spectral half-width	35 Å
Minimum integration time	20.8 ms
Best spatial resolution	0.36 deg

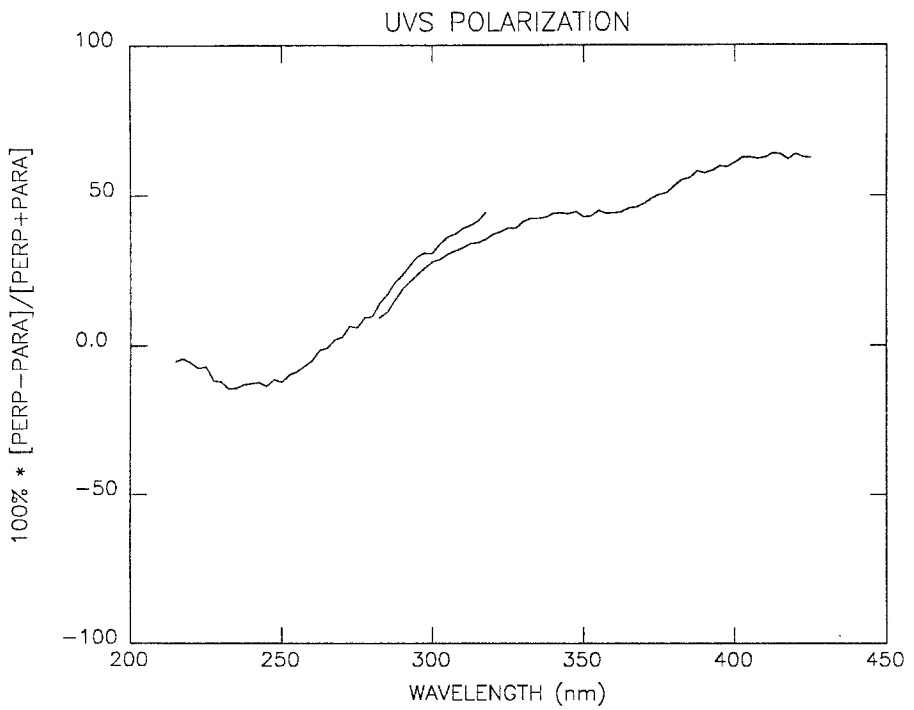

Fig. 8. The percent polarization for the UVS *F* and *N* channels. Perp and para are the response for the instrument to plane-polarized light which has the electric vector perpendicular and parallel to the UVS grating grooves, respectively. Differences in the measured polarization arise chiefly from the fact that the angles of incidence and diffraction for a single wavelength of light are different for the two detectors because their exit slits are located at different places in the spectrometer focal plane. Small differences may also arise from the additional optical elements in the *F* channel light path.

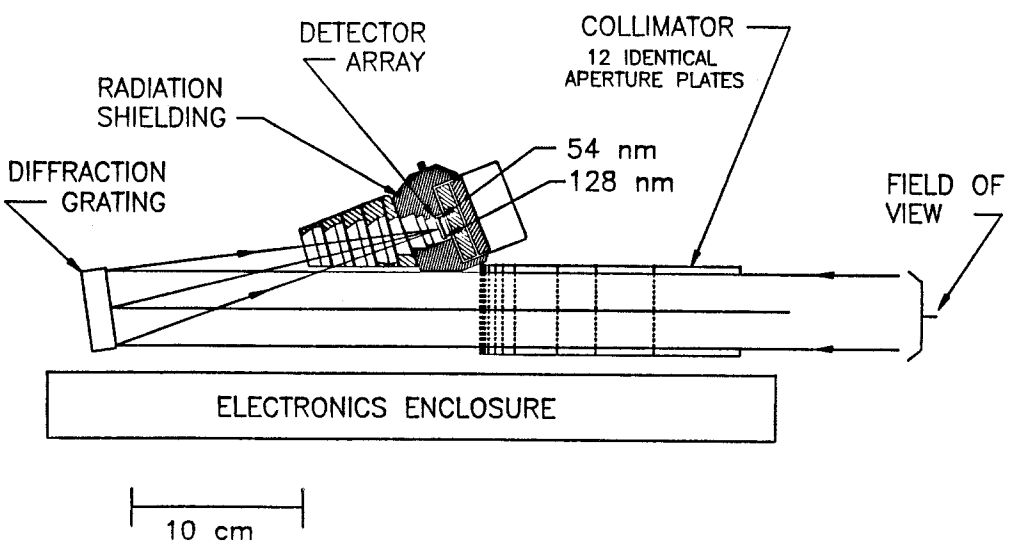

Fig. 9. EUVS mechanical-optical configuration.

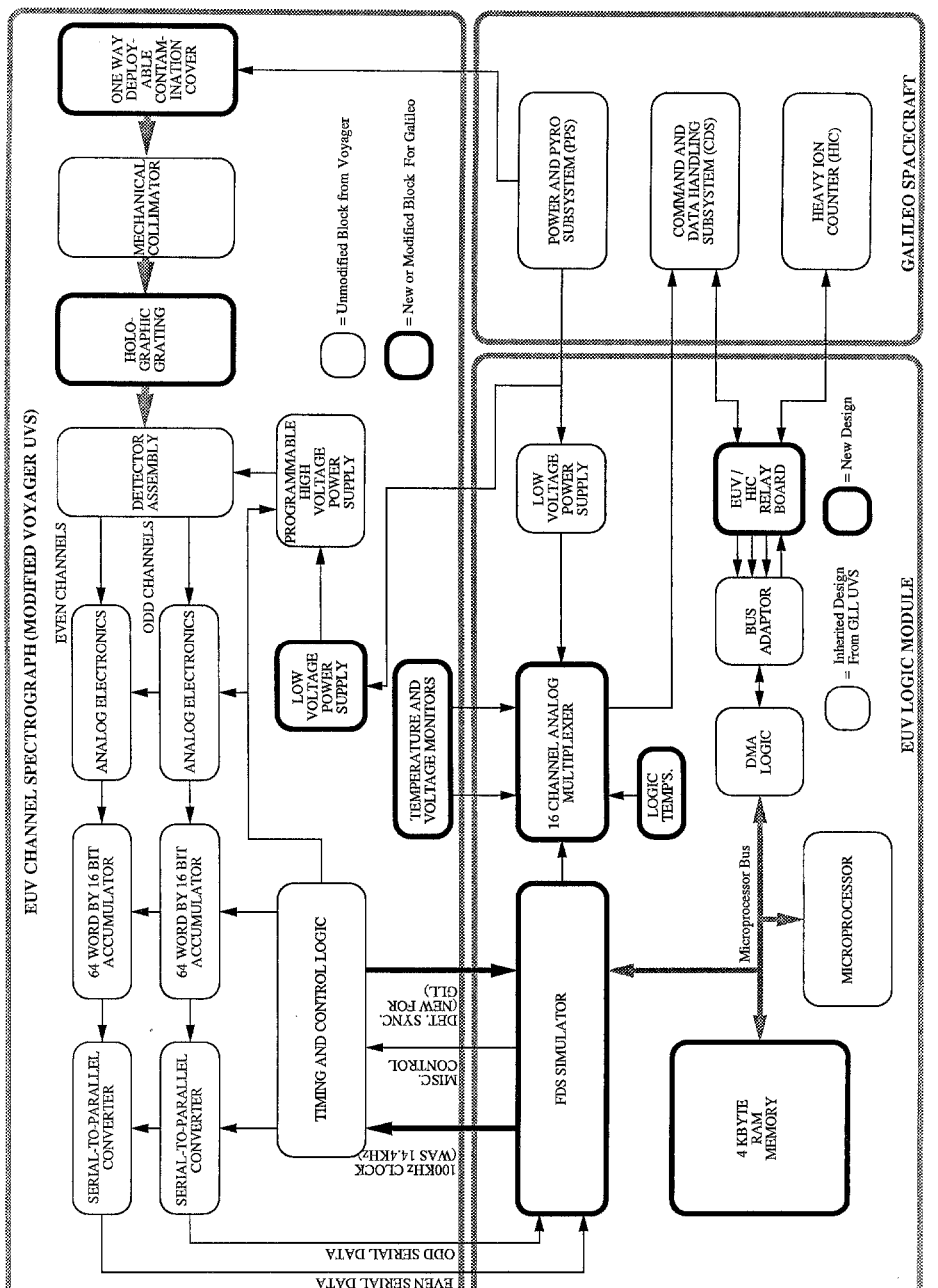

Fig. 10. EUVS functional block diagram.

extent. In practice, separation of spectral features from the scattering background is reasonably straightforward.

The collimator restricts the field of view in the dispersion direction to 0.17° FWHM, but is essentially open in the cross-dispersion direction; the field of view in this long direction is defined by the angular width of the detector in the image plane and is about 0.87°. The 40 × 60 mm diffraction grating has a spherical radius of curvature of 400.1 mm. The grating was fabricated holographically, and includes corrections to flatten the field at the image plane. The surface is coated with iridium to enhance the EUVS reflectivity. The dispersion required to match the desired wavelength range to the length of the detector is 5.9 nm mm^{-1}, which implies a ruling density of 851 lines mm^{-1}.

The instrument has two distinctly different spatial and spectral resolutions depending on the nature of the source. (1) An extended line emission source, which fills the field of view of the instrument, produces a triangular intensity distribution in the image plane 0.17° in half-width; this corresponds to a spectral half-width of 35 Å. (2) A point source is accurately imaged in the image plane and the width of a detector element, 0.029°, determines both the spectral and spatial resolutions. Both spatial and spectral resolution may be improved to some extent through spectral analysis.

4.2. Detector

The photon-counting detector uses a 128-element, linear, self-scanned anode array to collect the output of a dual microchannel plate (MCP) electron multiplier. This detector was developed for the Voyager instrument (Broadfoot and Sandel, 1977). The 128 narrow aluminium anodes, each 3 mm long, are deposited on 0.1-mm centers for a total collecting length of 13 mm in the dispersion direction. The specially designed 18-mm diameter MCPs have a rectangular active area corresponding to the collecting area of the anode array. Photons diffracted by the grating to the detector eject photoelectrons from the MCP. These photoelectrons undergo about 10^6 amplification through the cascaded microchannel plates. The pulse of electrons falls on the self-scanned anode array where the charge is stored. The anodes are accessed sequentially by a shift register and FET switches contained in the single integrated circuit. The scanning circuitry discharges each anode into a charge sensitive amplifier. If the charge pulse exceeds a fixed threshold, the memory location corresponding to the anode is incremented. The access time is 320 ms per anode; therefore, single random photo events can be recorded on any one of the 128 anodes with a rate of about 300 per second on each anode with a coincidence loss of about 10% of the events; such a loss can be corrected statistically. This is a satisfactorily high rate for the emissions from Jupiter and the plasma torus.

4.3. Calibration and sensitivity

The EUVS channel was calibrated in the EUVS Calibration Facility of the Lunar and Planetary Laboratory (LPL), and cross checked with the UVS at the Laboratory for Atmospheric and Space Physics (LASP).

LPL's EUVS Calibration Facility consists of a vacuum chamber with a gimballed

support for the instrument. The gimbal system can rotate the instrument about two perpendicular axes and translate it in a plane perpendicular to the UV beam. Light from a DC glow discharge enters a modified Seya–Namioka monochromator that selects the wavelength and collimates the exit beam. The dispersed and collimated beam enters the test chamber. Here a portion is split off to a channeltron and a portion continues to the instrument under test. The channeltron monitors the beam intensity continuously during the time that the spectrum is integrated within the EUVS.

The source, monochromator, and test chamber are differentially pumped, because no window materials can be used to separate them. Pumping is by a combination of turbo-molecular, ion, and cryogenic pumps. All these are oil-free systems suitable for use with microchannel plates and EUVS optics.

A second channeltron whose response over the wavelength range of the EUVS channel is known by calibration traceable to the National Bureau of Standards can be substituted in the position of the test instrument. It is used to map the intensity of the beam, and to thereby determine the absolute photon flux into the entrance aperture of the instrument. A microcomputer controls most aspects of the operation of the calibration system and acquires data from the EUVS channel and system monitors.

An important goal of the calibration procedure was to determine the absolute response of the EUVS channel as a function of wavelength. Other important goals were to measure the shape and width of the nominally triangular response function of the collimator, and to characterize the response to scattered light. The first is needed to combine with the on-axis response to compute the sensitivity to a uniformly bright monochromatic source filling the field of view. The second is needed to compute the effects of scattering from a bright emission line when it is necessary to measure nearby weak emissions superimposed on the scattering background (Holberg, 1986). Because the response of a single channel 100 Å from the peak signal to scattered light is only 1 to 2% of the total signal, substantial integration time was required to adequately determine the scattering characteristics.

The counting rate summed over all channels for a 1-Rayleigh monochromatic source filling the field of view is given by Equation (1).

$$C = I\omega A Q_e . \tag{1}$$

For the EUVS instrument ω, A, and Q_e have the following definitions: ω = angular field of view, $0.87° \times 0.34°$, or 9.3×10^{-5} steradian; A = ruled area of the grating, 21.2 cm^2; Q_e = transmission of the collimator, 0.33 × grating efficiency × detector quantum efficiency.

The sensitivity as a function of wavelength for this geometry (a uniform, extended monochromatic source filling the field of view) is shown by the solid line in Figure 11. Because of the triangular transmission function of the collimator, radiation from a monochromatic extended source incident on the detector will fall in a triangular intensity distribution over 12 anodes. The triangular half-width of six anodes will receive 75% of the signal. For an extended source emitting a continuum of wavelengths with

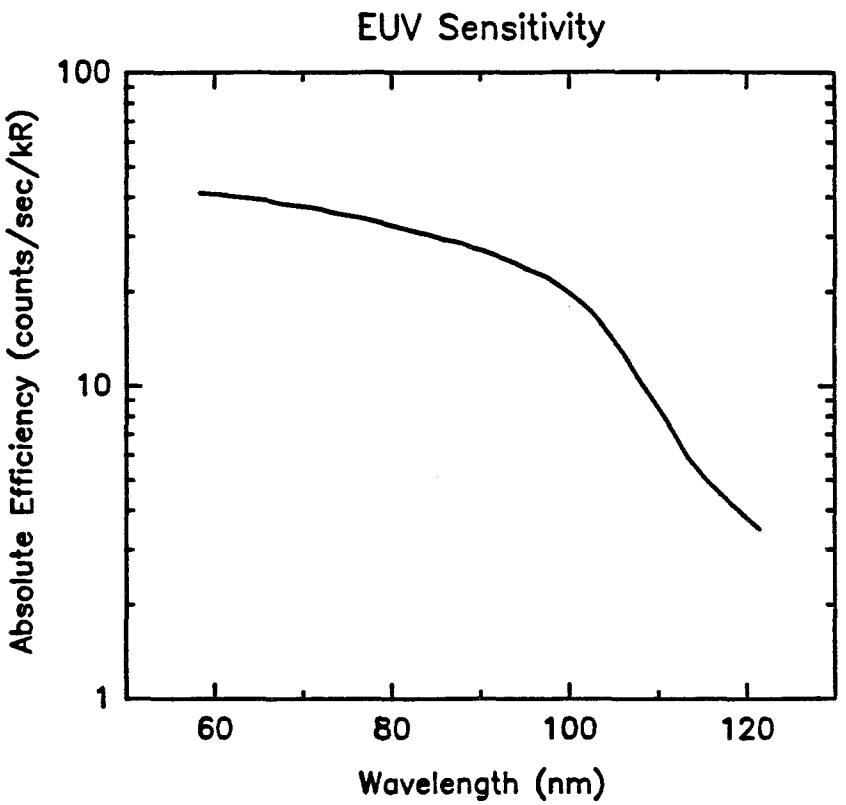

Fig. 11. EUVS sensitivity in counts per second per Rayleigh for a monochromatic emission line which fills the field of view. When the source radiance is expressed in Rayleighs per nanometer, the sensitivity must be multiplied by 3.5.

brightness 1 Rayleigh per nm, the count rate for a single anode is given by

$$C \times W, \tag{2}$$

where W is the spectral half-width, 3.5 nm.

The practical lower limit for the signal measurable by the EUVS channel is a function of both the instrument sensitivity and the dark count rate of the detector. An important advantage of the EUVS detector is its extremely low intrinsic dark count rate of less than 3×10^{-3} count anode^{-1} s^{-1}. In flight, this low dark count rate will not be realized because of noise induced by gamma rays from the RTGs. Our experience with Voyager has shown a dark count rate of 0.02 counts channel^{-1} s^{-1}, and on Galileo the dark count rate will probably be similar.

When the spacecraft is within about 15 R_J of Jupiter, noise induced by high-energy electrons trapped in the Jovian magnetic field will greatly exceed the intrinsic noise of the detector. Extensive shielding has been provided around the detector to reduce radiation interference.

4.4. Data handling and spacecraft interface

To ease the adaptation of the Voyager instrument to the Galileo spacecraft, changes to the spectrograph enclosure were minimized, and an external logic box to interface the EUVS spectrograph and electronics to the Galileo bus was constructed.

This design restricts the rate at which the spectrum can be read from the EUVS memory to 20.8 ms. During this time, the spacecraft will rotate by 0.37°, which defines the spatial resolution in the roll (dispersion) direction.

Because of its late addition to the spacecraft, the EUVS channel shares a telemetry channel with the Heavy Ion Counter (HIC). We have implemented a procedure in the logic box that time-tags detected photons as the information is read from the memory in the spectrograph enclosure. The procedure is based on the concept of a sector. A sector is a time corresponding to an integral number n of 20.8-ms intervals, or equivalently, a number n 0.37° sections of the band swept out on the sky by the EUVS field of view. The number n is programmable. For encounter operations, it will usually be 1 to give the best available spatial resolution, but for cruise observations it may be much larger. The crossing of sector boundaries is marked in the telemetry stream by a unique byte. Between sector boundaries, the wavelength position of each photo event recorded in the spectrograph memory is telemetered. Synchronizing the sector boundaries with spacecraft roll phase then permits reconstruction, on the ground, of the wavelength and origin on the sky of each detected photon.

To remain within the allocated telemetry rate, during encounter operations it will be necessary to restrict processing of data to that portion of the roll when Jupiter and the plasma torus are in the EUVS field of view.

Two additional data buffers will be used during encounter and orbit operations. The first of these, called the wavelength buffer, is a 128-element buffer that accumulates the spectrum over all sectors. The second, the sector buffer, has an element corresponding to each of the sectors and sums all photo events detected in a particular sector into the appropriate element. Thus data in the wavelength buffer represent the spectrum averaged over all sectors, and data in the sector buffer represent the spatial variation in the intensity summed over the passband of the EUVS channel.

Cruise observations will consist mainly of mapping He 58.4 nm and H Lα emissions from the local interstellar medium. For this investigation, it is desirable to record data over the full range of roll phase, but high spatial resolution is less important than for encounters.

4.5. EUVS logic module

The EUVS uses an RCA 1802 CMOS microprocessor for command parsing, spacecraft time and sector recognition and synchronization, and instrument control. The microprocessor and support logic, the bus adaptor, and the DMA logic are identical to that for the UVS. New designs were required for a 4 kbyte Random Access Memory (RAM) and a simulator for the Flight Data System (FDS) from the Voyager spacecraft. The simulator allowed us to transform the data from the EUVS channel to the Galileo spacecraft without modifying the original Voyager-style hardware.

The EUVS Microprocessor Logic differs from the UVS in two ways: (1) there is no Cold Start Mode, and (2) the microprocessor is responsible for data buffering, formatting, and transmission from the EUVS channel Spectrometer to the Galileo Command and Data System (CDS). It receives commands, and spacecraft timing and sector information via the Bus Adaptor and associated Direct Memory Access (DMA) logic. The DMA logic also handles the function of loading and verifying program memory, and of reading out telemetry data from the microprocessor telemetry data buffer.

The FDS Simulator performs all interface tasks to simulate the Voyager FDS including gated clocks, discrete I/O, and serial-to-parallel conversion of the two EUVS channel data lines. This logic also contains the handshaking circuitry necessary to achieve 20.8 ms integration periods.

The Bus Adaptor serves as the bi-directional interface between the Galileo spacecraft and the EUVS. The spacecraft bus is defined to contain four signals. These include a 806.4 kHz clock, the Real Time Interrupt (RTI) timing signal, and one line for serial communications in both directions. The bus adaptor circuitry serves to electrically isolate the EUVS from the spacecraft, and to allow for 8-bit information flow to and from the EUVS.

4.6. Operational modes and microprocessor software

The EUVS software supports two distinct operational modes. These modes are defined as: (1) encounter mode, and (2) cruise mode. Encounter mode is the primary science mode, and will be utilized when the spacecraft is in the Jovian environment. Cruise mode provides monitoring of EUVS sources while the spacecraft is traveling to Jupiter.

4.7. Encounter mode

The EUVS software includes two, 1 kbyte buffers (Encounter Mode only). The first, called the Pixel Data Buffer (PDB), is a circular buffer which holds data from the EUVS channel Spectrometer. Data is placed in this buffer whenever the FDS Simulator detects non-zero data. The second circular buffer, called the Spin Packet Buffer, is filled as the microprocessor removes data from the PDB in non-real time and transforms this data into the Galileo EUVS format. Twelve bytes are removed from this buffer every $\frac{2}{3}$rd s.

Because of the spinning motion, the microprocessor must monitor the spin position and gate the integration periods as the EUVS field of view sweeps past its target. This is accomplished by monitoring the spacecraft sector broadcasts. The minimum integration time corresponds to 0.3744°.

The following four parameters for the EUVS can be set by spacecraft command: (1) High voltage level applied to the microchannel plates to select the gain of the detector. (2) The roll angle at which integration should start. This fixes the start angle granularity to approximately 1.4°. (3) and (4) establish the time of integration, i.e., the angle over which the instrument will integrate. When the EUVS detects photons, it basically time tags the photons, so that when combined with the roll position, the photons can be linked to specific physical locations in the sky. The third parameter determines the minimum angular resolution over which target is subdivided, and defines

the number of 20.8 ms (0.3744°) periods to integrate before incrementing the time tag. This parameter is called an EUVS Sector. The fourth parameter sets the total time the EUVS integrates each spin, by defining the number of EUVS Sectors that make up an integration period. Thus the total integration period is equal to 20.8 ms × parameter 3 × parameter 4.

The EUVS is body fixed on the spinning section of Galileo with its field of view pointing at right angles to the spin axis. Figure 12 is a schematic of the observing

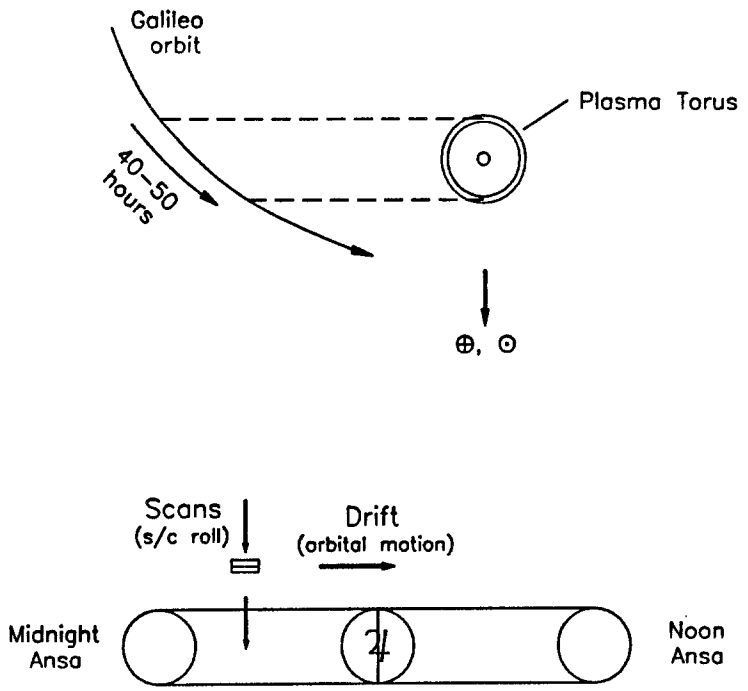

Fig. 12. *Top*: A schematic representation of a typical Galileo orbit, approximately to scale, as seen from above Jupiter's north rotation pole. Galileo's roll axis is pointed toward Earth, and the dashed lines show the positions at which the EUVS field crosses the ansas of the torus. *Bottom*: A schematic view of the plasma torus and Jupiter as seen from Galileo at an orbital position between the two dashed lines in the top panel. The EUVS instantaneous field is shown by the small lower rectangle; the spatial resolution implied by the minimum sector size is represented by the larger rectangle.

geometry. The orbital motion of Galileo carries the field of the EUVS across the plasma torus and Jupiter twice in each orbit. Because the spin axis points toward Earth, and therefore nearly toward the Sun, one of these sweeps occurs when Galileo is near Jupiter's dawn meridian, and the other when it is near dusk. Only the sweep near the dawn meridian is useful for the EUVS, because a typical orbit carries the spacecraft inside 25 R_J at the dusk meridian crossing where high radiation-induced dark counts will mask the data.

For a typical orbit, the EUVS field crosses the torus from ansa to ansa in about

45 hours, at a rate of about 0.3 R_J per hour. The spatial resolution element will be about 0.75 R_J parallel to the orbital plane of the satellites, and about 0.32 R_J perpendicular to the plane. Thus there will be about 6 resolution elements across the torus and from pole to pole on Jupiter. The spacecraft rolls some 450 times as the EUVS field moves by its own length parallel to the satellite plane. Thus, for some of the brighter emissions, it should be possible to detect spatial structure having scales smaller than the 0.75 R_J length of the slit.

4.8. Cruise mode

The mechanism for telemetering data in cruise is to use trickle memory readouts at about 15 bps. By using larger values in parameters 3 and 4, brightness measurements can be recorded at most values of the roll phase.

A single 1.5 kbyte telemetry buffer is read out. The contents of the buffer is a two-dimensional array, e.g., the first index defining an EUVS sector, and the second index defining a given pixel number (i.e., wavelength).

Whenever the FDS Simulator detects non-zero data, the appropriate register in the two-dimensional array is modified to include these data. Thus the value of each element in this array is the accumulation of photo events at a given wavelength in a particular section of the sky.

Acknowledgements

We would like to thank the many people who supported the addition of the Extreme Ultraviolet Spectrometer to the Galileo Orbiter science payload. Of the EUV's many fathers, we would like to single out John Casani for his support and confidence in our team.

References

Ajello, J. M., Shemansky, D. E., Franklin, B., Watkins, J., Srivastava, S., James, G. K., Simms, W. T., Hord, C. W., Pryor, W. R., McClintock, W. E., Argabright, V., and Hall, D.: 1988, *Appl. Optics* **27**.

Beebe, R. F., Orten, G. S., and West, R. A.: 1989, NASA Special Publication SP-494, p. 245.

Beutler, H. G.: 1945, *J. Opt. Soc. Am.* **35**, 311.

Broadfoot, A. L. and Sandel, B. R.: 1977, *Appl. Optics* **16**, 1533.

Broadfoot, A. L., Sandel, B. R., Shemansky, D. E., Atreya, S. K., Donahue, T. M., Moos, H. W., Bertaux, J. L., Blamont, J. E., Ajello, J. M., Strobel, D. F., McConnell, J. C., Dalgarno, A., Goody, R., McElroy, M. B., and Yung, Y. L.: 1977, *Space Sci. Rev.* **21**, 183, 205.

Caldwell, J., Cess, R. D., Carlson, B. E., Tokunaga, A. T., Gillet, F. C., and Nolt, I. G.: 1979, *Astrophys. J.* **234**, L155.

Clarke, J., Caldwell, J., Skinner, T., and Yelle, R.: 1989a, NASA Special Publications SP-494, p. 211.

Clarke, J. T., Trauger, J., and Waite, J. H., Jr.: 1989b, *Geophys. Res. Letters* **16**, 587.

Eshleman, V. R., Tyler, G. L., Wood, G. E., Lindal, G. F., Anderson, J. D., Levy, G. S., and Croft, T. A.: 1979, *Science* **204**, 976.

Fastie, W. G., Feldman, P. D., Henry, R. C., Moos, H. W., and Donahue, T. M.: 1973, *Science* **182**, 710.

Geirasch, P. J., Conrath, B. J., and Mahalhães, J. A.: 1986, *Icarus* **67**, 456.

Gladstone, G. R. and Skinner, T. E.: 1989, NASA Special Publication SP-494, p. 221.

Hale, G. E. and Wadsworth, F. L. O.: 1896, *Astrophys. J.* **4**, 54.

Hall, D. and Shemansky, D. E.: 1988, *Nature* **335**, 417.
Holberg, J. B.: 1986, *Astrophys. J.* **311**, 969.
Lawrence, G. M., Barth, C. A., and Argabright, V.: 1977, *Science* **195**, 573.
McClintock, W. E., Barth, C. A., Steele, R. E., Lawrence, G. M., and Timothy, J. G.: 1982, *Appl. Optics* **21**, 3071.
Metzger, A. E., Gilman, D. A., Luthey, J. L., and Hurley, K. C.: 1983, *J. Geophys. Res.* **88**, 7731.
Stewart, A. I. and Barth, C. A.: 1979, *Science* **205**, 59.
Strobel, D. F.: 1975, *Rev. Geophys. Space Phys.* **13**, 372.
Strobel, D. F.: 1989, NASA Special Publication SP-494, p. 183.
Thomas, G. E.: 1978, *Ann. Rev. Earth Planetary Sci.* **6**, 173.